Scientific
Research

Photoluminescent Properties of CoMoO$_4$ Nanorods Quickly Synthesized and Annealed in a Domestic Microwave Oven

Ana P. de Moura[1], Larissa H. de Oliveira[2], Paula F. S. Pereira[2], Ieda L. V. Rosa[2*], Máximo S. Li[3], Elson Longo[1], José A. Varela[1]

[1]Chemistry Institute, University of Sao Paulo State, Araraquara, Brazil
[2]Chemistry Department, Federal University of Sao Carlos, São Carlos, Brazil
[3]Physical Institute, University of Sao Paulo, São Carlos, Brazil
Email: *ilvrosa@ufscar.br

ABSTRACT

A simple way to prepare α- and β-CoMoO$_4$ nanorods is reported in this paper. CoMoO$_4$·xH$_2$O nanorod precursors were obtained using the microwave-assisted hydrothermal (MAH) method. By annealing the as-prepared CoMoO$_4$·xH$_2$O precursor at 600˚C for 10 min in a domestic microwave oven, α- and β-CoMoO$_4$ nanorods were prepared. These powders were analyzed by X-ray diffraction (XRD), field emission scanning electron microscopy (FE-SEM), Fourier transform Raman microscopy and ultraviolet visible absorption spectroscopy (UV-vis spectra) as well as photoluminescence (PL) measurements. Based on the results, these materials revealed nanorod morphology. PL spectra obtained at room temperature for α- and β-CoMoO$_4$ particles exhibited maximum components around the blue light emission. The results show that the domestic microwave oven has been successfully employed to obtain α- and β-CoMoO$_4$ nanoparticles.

1. Introduction

Materials belonging to the molybdate and tungstate families have a long history of practical applications due to their excellent optical properties in phosphors, laser materials, and scintillation detectors [1-3].

Tungstate and molybdate based materials with a schelite-type structure, have molybdenum (or tungsten) atoms in a tetrahedral coordination as well as large bivalent cations (ionic radius > 0.99 Å such as Ca, Ba, Pb and Sr) as lattice modifiers [4]. However, when the modifier atoms are small bivalent cations (ionic radius < 0.77 Å; e.g., Fe, Mn, Co, Ni, Mg and Zn), the tungstate and molybdate-based materials have a wolframite-type structure where the molybdenum (or tungsten) atom adopts an overall six-fold coordination [5,6].

Among these materials, cobalt molybdate (CoMoO$_4$) is one of the most important components of industrial catalysts for the partial oxidation of hydrocarbons and precursors in the synthesis of hydrodesulphurization catalysts [7-9]. In addition, CoMoO$_4$ can also be applied in the electronics and bioscience industries due to its structural, magnetic, electronic and antibacterial properties

[9-17]. Therefore, four stoichiometric type CoMoO$_4$ crystalline structures are reported by the literature. The phase α-CoMoO$_4$ was verified at low temperatures [18]; at high temperatures, the β-CoMoO$_4$ phase was stable [19] while at high pressures, the hydrated phase (CoMoO$_4$·xH$_2$O) is the more stable phase [10].

In recent years, different chemical methods have been employed to synthesize CoMoO$_4$ powders such as solid state reaction [18,20], co-precipitation [21], sol-gel [22] and hydrothermal methods [14], etc. However, some of these methods require long annealing times and result in higher costs [23] as well as other disadvantages such as the formation of a large amount of organic waste, polydisperse particles sizes and an undefined morphology.

Komarneni *et al*. [24,25] combined microwave radiation with the hydrothermal system to synthesize ceramic powders. The use of microwave energy in a conventional hydrothermal system promoted the development of a new technique which facilitated rapid heating and rates of crystallization [26]. Thus, the MAH method can be employed as an efficient synthesis route in processing materials due to rapid kinetics which accelerates the crystallization process through the enhancement of the nucleation

rate. In this method, chemical reaction is related to the effect of microwave radiation during the experimental procedure which interacts with the permanent dipole of the solvent and induces molecular vibration and promotes rapid heating as a result of molecular rotation [27].

Therefore, in this study, $CoMoO_4 \cdot xH_2O$ precursors were prepared by the MAH method and then heat treated using microwave radiation to form the desired α- and β-$CoMoO_4$ phases. These materials were chemically, structurally and morphologically investigated by XRD, FE-SEM, (UV-vis) and Raman spectroscopy; their optical properties were also investigated by PL measurements at room temperature.

2. Experimental Section

2.1. Synthesis of the Precursors

In a typical procedure, 2 mmol of sodium molybdate solution was dissolved in 50 mL of distilled water. Then, 2 mmol of cobalt nitrate hexaydrate was dissolved in 50 mL of deionized water which was slowly added to the sodium molybdate solution under magnetic stirring which produced a homogeneous solution (pH = 6). The reaction mixture was transferred to a Teflon-lined stainless autoclave which was finally sealed and placed in the MH system using 2.45 GHz microwave radiation with maximum power of 800 W. MH conditions were kept at 140°C for 1, 2, 4, 8, 16 and 32 minutes. Then, the autoclave was naturally cooled to room temperature. These as-prepared purple precursor powders were labeled as P1, P2, P4, P8 P16 and P32, respectively. Precursors P1, P2, P4, P8, P16 and P32 were water washed several times until a neutral pH was obtained and then dried at 60°C for 8 h under atmospheric air in a conventional furnace.

2.2. Synthesis of α- and β-$CoMoO_4$ Powders

$CoMoO_4$ powders were obtained from the thermal decomposition of precursors P1, P2, P4, P8, P16 and P32. These precursor powders were placed in ceramic crucibles and heated in a microwave sintering furnace at 600°C for 10 minutes. The calcinated brown-like powders were labeled D1, D2, D4, D8 D16 and D32 samples, respectively.

2.3. Characterizations

Precursors P1, P2, P4, P8 P16 and P32 and α- and β-$CoMoO_4$ powders D1, D2, D4, D8 D16 and D32 were characterized by powder XRD using a Rigaku-DMax 2500PC, (Japan) with Cu Kα radiation ($\lambda = 1.540598$ Å) in the 2θ range from 5° to 75° using a scanning rate of 0.02°/min. The morphologies of the samples were verified using FE-SEM (Jeol JSM 6330F). The particle size of precursors and $CoMoO_4$ powders were determined

using FE-SEM images and were calculated using the Image J. program. UV-vis spectra were taken using Cary 5G (Varian, USA) equipment in the diffuse reflection mode. The thermal decomposition of the precursor powders was studied by thermogravimetric analysis (TGA/DTA) on a TGA 2050 thermal analysis device (American TA Corporation). TGA determination was carried out in air at a heating rate of $20°C/min^{-1}$ in the range from room temperature to 900°C.

PL precursor measurements were taken in a Thermal Jarrel-Ash Monospec 27 monochromator and a Hamamatsu R446 photomultiplier. The 350.7 nm exciting wavelength of a krypton ion laser (Coherent Innova) was used with the nominal output power of the laser power kept at 200 mW. All the measurements were taken at room temperature.

3. Results and Discussion

3.1. Precursor Nanorods

3.1.1. XRD Patterns of the Precursor Nanorods

Figure 1 shows XRD patterns of precursor P1 from MAH processing at 140°C for 1 minute. The results revealed that MAH treatment led to the formation of a pure phase $CoMoO_4 \cdot xH_2O$ with good crystallinity (see **Figure 1**).

All reflection peaks of different samples prepared at different times can be easily indexed as the $CoMoO_4 \cdot xH_2O$ phase of the purple powders. The formation of $CoMoO_4 \cdot xH_2O$ pure powders with a monoclinic structure and cell parameters of $\alpha = 9.501$ Å, $b = 8.897$ Å, $c = 7.751$ Å and $\beta = 113.83°$ (Joint Committee on Powder Diffraction Standards (JCPDS) N°. 26-0477) was verified. These observations confirm that MH processing results in the formation of a product based on XRD patterns of the as-prepared P1 powder obtained from the MAH method at 140°C for 1 min.
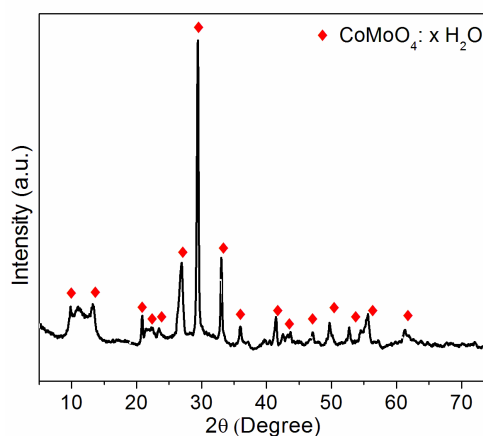

Figure 1. XRD patterns of the precursor P1 microwave-hydrothermal assisted at 140°C for 1 minute.

3.1.2. FE-SEM Images of the Precursors Nanorods

Figure 2(A) shows FEG-SEM images of the P1 powders. This sample consists of large-scale and homogeneous CoMoO$_4$·xH$_2$O particles with morphology-like nanorods. This morphology was observed for all P1, P2, P4, P8 P16 and P32 precursors. **Figure 2(B)** is a histogram with the calculated average thickness of these nanorods evaluated as 100 - 300 nm. Nanorods lengths were determined as *ca.* 1 - 3 μm. All other samples prepared at different times showed similar morphology.

3.1.3. TGA Curves of Precursor Nanorods

The thermal behavior of the P1 precursor nanostructure was examined by TGA measurements (see **Figure 3**).

The TGA curve shows that the precursor decomposition occurs in two steps: 1) in a temperature range of 84˚C and 165˚C; and 2) between 168˚C and 450˚C. A total weight loss of 5.75% was obtained which, according to Ding and co-workers [6], is largely ascribed to water loss corresponding to the water content in the hydrated product. These researchers also observed these two steps where the desired CoMoO$_4$ crystalline structure occurred at 45˚C. Thus, the 600˚C temperature was chosen to heat treat precursor powders to obtain the pure CoMoO$_4$.
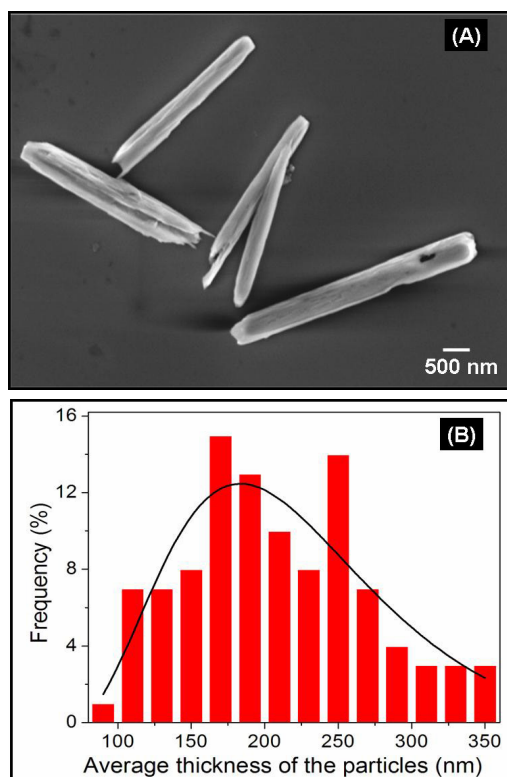

Figure 2. (A) FEG-SEM micrographies images and (B) average thickness distribution of the particles (nm) of the CoMoO$_4$·xH$_2$O powder obtained by the microwave-hydro-thermal assisted method (MH) at 140˚C for 1 min (P1).

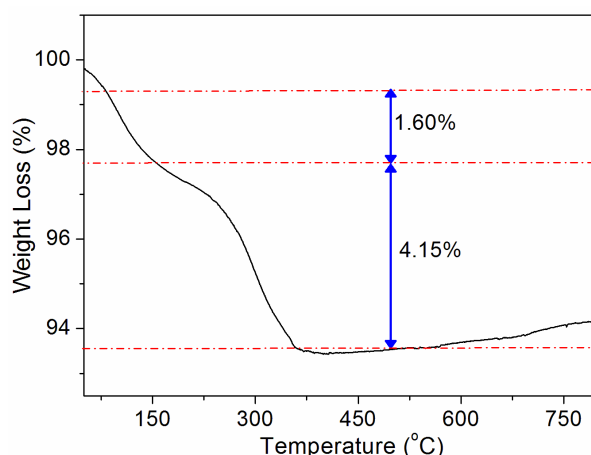**Figure 3. TGA curves of the as-prepared CoMoO$_4$·xH$_2$O precursor powder obtained from by the microwave-hydro-thermal assisted method (MH) at 140˚C by 1 min.**

3.2. α- and β-CoMoO$_4$

3.2.1. XRD Patterns of α- and β-CoMoO$_4$ Powders

XRD patterns of α- and β-CoMoO$_4$ phases obtained by thermal decomposition of the precursor (CoMoO$_4$·xH$_2$O) are shown in **Figure 4**.

XRD patterns reveal that all calcined samples have well defined narrow diffraction peaks of two phases that are ordered at long range. α-CoMoO$_4$ has a monoclinic structure with a space group of C2/m (Joint Committee on Powder Diffraction Standards) (JCPDS N˚. 25.1434), and β-CoMoO$_4$ has a monoclinic structure with a space group of C2/m (JCPDS No. 21-0868), respectively.

3.2.2. Raman Spectra of α- and β-CoMoO$_4$ Powders

Figure 5 shows Raman spectra of D1, D2, D4, D8 D16 and D32 samples, respectively. Raman spectra collected at room temperature showed that both α and β phases have similar vibrational modes related to the CoMoO$_4$ with a space group of C2/m. These vibrational modes are observed at 330, 369, 698, 815, 879, and 941 cm^{-1}. The Raman mode at 941 cm^{-1} is associated with the symmetric stretching mode of Mo-O. The bands located at 879 cm^{-1} and 815 cm^{-1} correspond to asymmetric stretching modes of oxygen in binding O-Mo-O. The bands observed at 330 cm^{-1} and 369 cm^{-1} are related to asymmetric and symmetric bending modes of the O-Mo-O, respectively. The band located at 698 cm^{-1} can be attributed to the symmetric stretching of the Co-O-Mo bond (see **Table 1**). **Figure 5** illustrates that all Raman spectra have the same features. The results obtained are in agreement with the literature [28], and the small variations in the positions of the vibrational modes can be associated with the method of preparation, crystal size, morphology and strength of interaction between the ions and the degree of structural order-disorder of these materials.
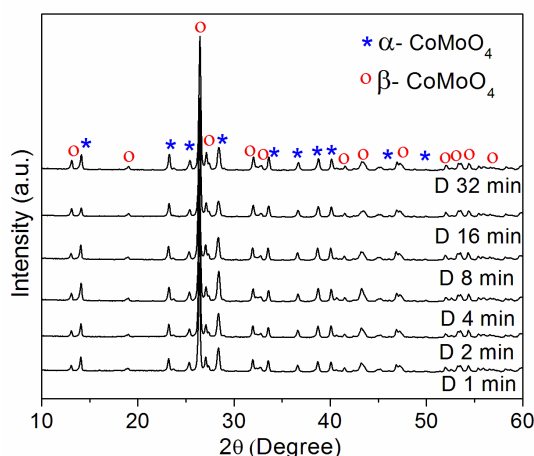
Figure 4. XRD patterns of the (a) D1, (b) D2, (c) D4, (d) D8, (e) D16 and (f) D32 powders prepared by thermal decomposition of the CoMoO$_4$·xH$_2$O precursors at 600°C for 10 minutes.
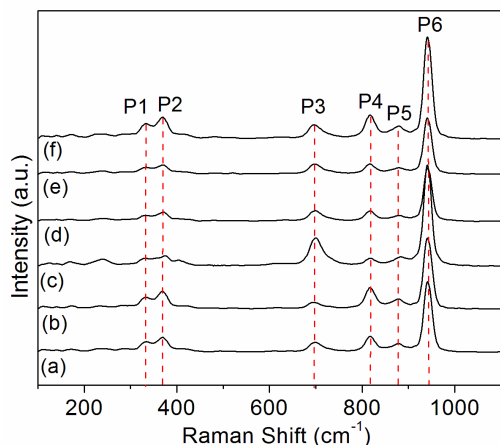

Figure 5. Raman spectra of the (a) D 1, (b) D 2, (c) D 4, (d) D 8, (e) D 16 and (f) D 32 samples.

Table 1. Relative positions of the Raman active modes for the samples of α- and β-CoMoO$_4$.

Symbol	Position	Vibrational Mode
P6	941 cm^{-1}	Symmetric stretch O-Mo-O
P5, P4	879 cm^{-1} e 815 cm^{-1}	Assimmetric stretch O-Mo-O
P3	698 cm^{-1}	Symmetric stretch Co-Mo-O
P2	330 cm^{-1}	Assimmetric torsional mode O-Mo-O
P1	369 cm^{-1}	Symmetric torsional mode O-Mo-O

3.2.3. FE-SEM Analysis of α- and β-CoMoO$_4$ Powders

Crystal structures of α- and β-CoMoO$_4$ rods annealed at 600°C were characterized by FE-SEM.

Figure 6 shows FE-SEM images of (a) D1, (b) D2, (c) D4, (d) D8, (e) D16 and (f) D32 powders, respectively.

The nanorod-like morphology of α- and β-CoMoO$_4$ was similar to the precursors (**Figures 2** and **6**) which indicate that this method is a good approach to prepare powders with controlled morphology.

Figure 7 shows the average thickness distribution of particles for samples (A) D1, (B) D2, (C) D4, (D) D8, (E) D16 and (F) D32. According to these graphics all particles have the same thickness being which is evaluated as *ca.* 250 and 350 nm. Particle lengths were determined to be between 2 to 4 μm.

3.3.4. Ultraviolet-Visible Absorption Spectroscopy Analyses

The optical energy gap is associated with the degree of structural order and disorder of the materials in a medium range. The order/disorder ratio leads to different defect densities in the material which results in different distributions of intermediate levels of energy between the valence (VB) and conduction band (CB). Most crystalline materials exhibit a greater degree of organization when compared to the less crystalline materials with more structural defects. Therefore, these materials exhibit a high optical energy gap value because they have small intermediate energy levels between the VB and CB [29].

The optical band gap energy (E_g) of α- and β-CoMoO$_4$ nanorods was estimated by the method proposed by Wood and Tauc [30]. According to these authors the E_g is associated with absorbance and photon energy by the following equation:

$$h\upsilon\alpha \propto \left(h\upsilon - E_g\right)^m, \tag{1}$$

where α is the absorbance, h is Planck's constant, υ is the frequency, E_g is the optical band gap and m is a constant associated with the different types of electronic transitions (m = 1/2, 2, 3/2 or 3 for direct allowed, indirect allowed, direct forbidden and indirect forbidden transitions, respectively). In this case, E_g values of the powders were evaluated by extrapolating the linear portion of the curve or tail. The m value suggested in our work is 2 which indicate an indirect allowed transition.

The Uv-vis absorbance spectra of the samples as well as the gap values are presented in **Figure 8**. The value of the Eg was quantified from spectra in **Figure 8**. Samples D1, D2, D4, D8, D16 and D32 have respectively gap values of 2, 1.8, 2.1, 2.1, 2.4, and 2.0 eV. The results obtained in this study are in accordance with the value of 1.8 eV already published [31]. The small difference in our results is probably due to quantum size effects as well as reaction conditions of the medium. Both effects promote different structural defects in the materials. The preparation time for precursors with microwave irradiation results changes E_g values. A pronounced difference between samples D2 min and D16 min is evident. According to another report [1], three different charge states

occurring in oxygen vacancies in molybdenum are $[MoO_3 \cdot V_O^X]$, $[MoO_3 \cdot V_O^{\cdot}]$, and $[MoO_3 \cdot V_O^{\cdot\cdot}]$ complex states. The $[MoO_3 \cdot V_O^X]$, complex state has two paired electrons ↑↓ and is a neutral relative to the lattice. The single ionized $[MoO_3 \cdot V_O^{\cdot}]$, complex state has one unpaired electron ↑, and the $[MoO_3 \cdot V_O^{\cdot\cdot}]$ complex state did not trap any electrons and was doubly positively charged with respect to the lattice. The authors speculate that these oxygen vacancies induced new energy in the band gap and were attributable to the molybdenum-oxygen complex vacancy centers. In this case, the interaction of these clusters with microwave irradiation results in distortions in the angles and lengths of bonds which generates different degrees of defects and different distributions of intermediate energy levels between VB and CB.

3.3.5. PL Measurements

Figure 9 illustrates PL spectra of D1, D2, D4, D8 D16 and D32 powders at room temperature using excitation of a krypton laser source at 350.7 nm. These PL spectra exhibited a broad band in the range of 300 - 600 nm which is ascribed to a multiphoton process where many intermediate levels of energy are involved in the PL process where relaxation occurs by several paths. PL spectra observed for all powders show a maximum emission located at 450 nm (blue region of the electromagnetic spectrum). According to Wu *et al.* [32,33], the emission band shape might be explained by considering the Jahn-Teller active vibration modes of T_2 symmetry that influence the $[MoO_4]^{2-}$ complex anion of slightly distorted tetrahedral symmetry which leads to a structured absorption band for the A_1-$T_{1(2)}$ transition.
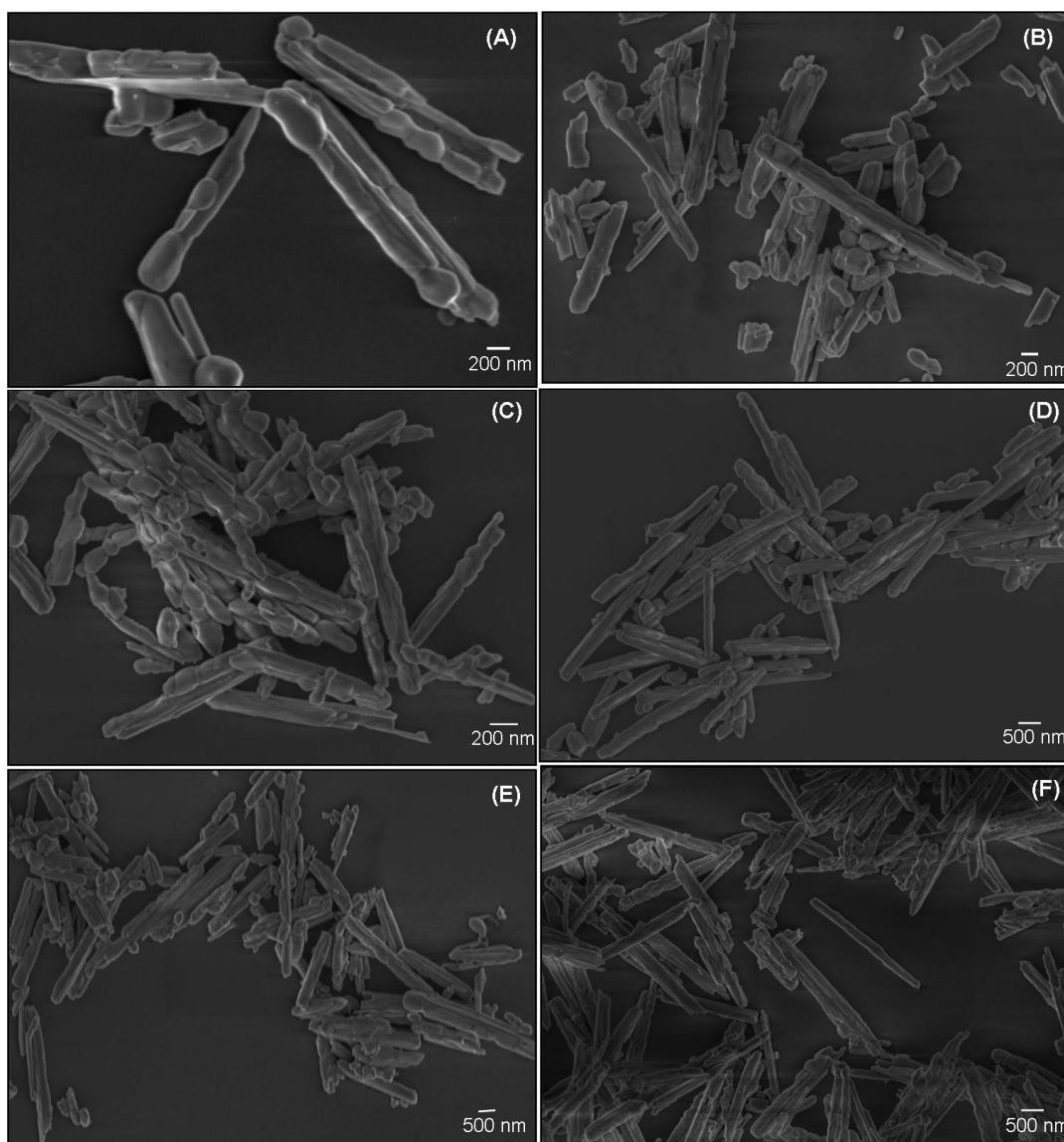

Figure 6. FE-SEM micrographies α- and β-CoMoO₄ samples: (A) D 1, (B) D 2, (C) D 4, (D) D 8, (E) D 16 and (F) D 32.
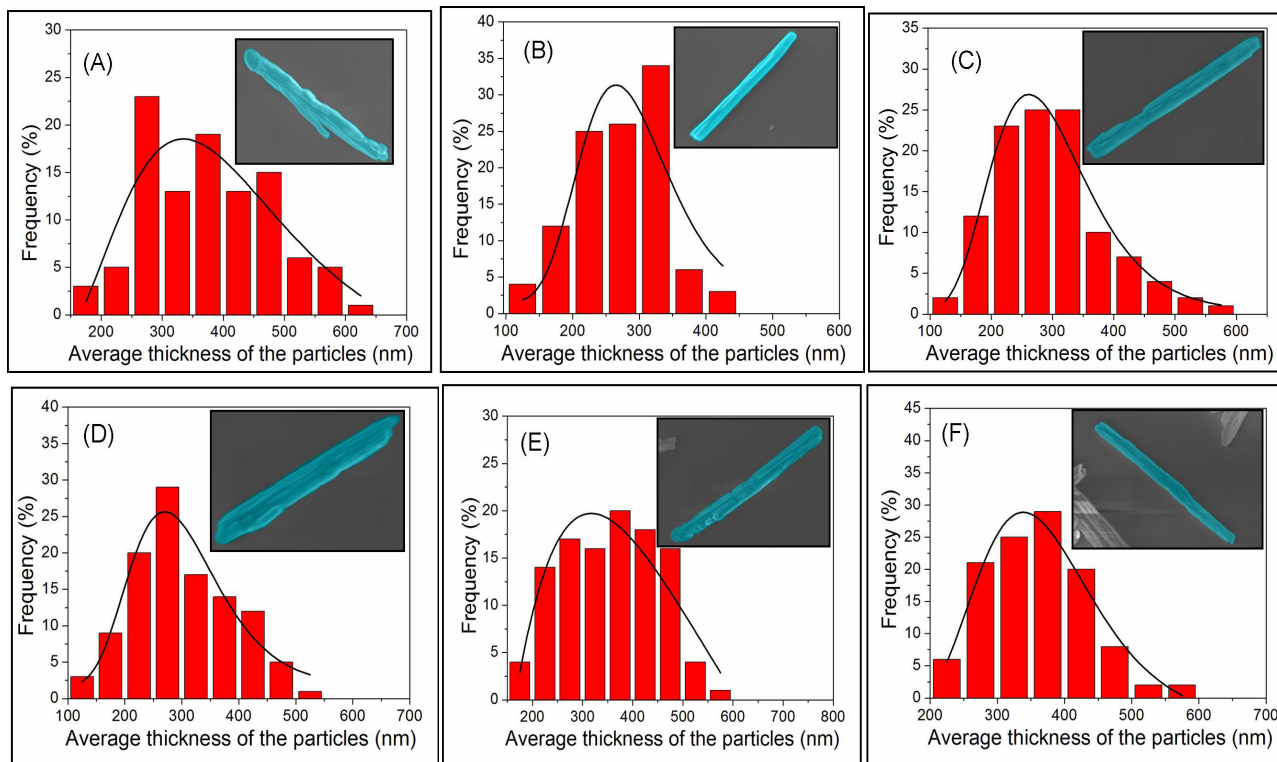
Figure 7. Average thickness distribution of the particles (nm) for the samples: (A) D1, (B) D2, (C) D4, (D) D8, (E) D16 and (F) D32.
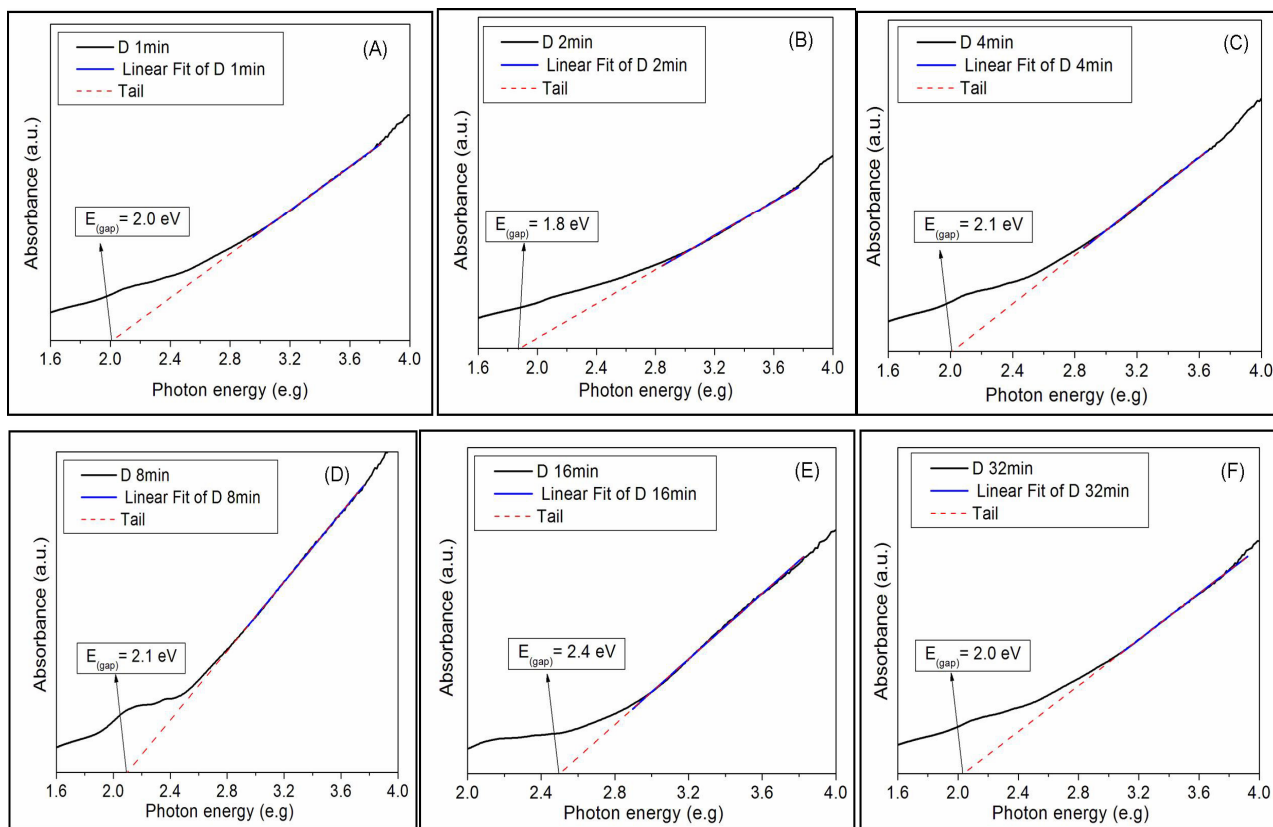

Figure 8. UV-vis absorbance spectra of the samples: (A) D1, (B) D2, (C) D4, (D) D8, (E) D16 and (F) D32.
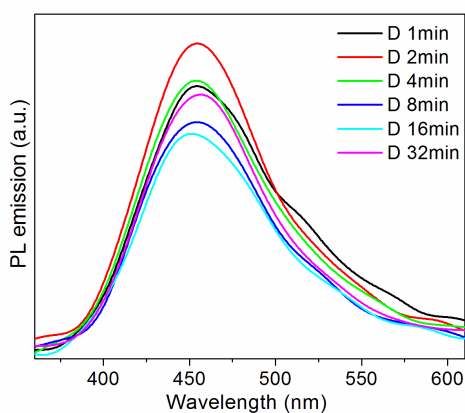
Figure 9. PL spectra of the samples α- and β-CoMoO₄: (A) D1, (B) D2, (C) D4, (D) D8, (E) D16 and (F) D32.

Figure 9 also shows that the precursor processing time influenced PL behavior due to the verified differences in emission intensities and a slight shift in the maximum intensities positions.

The PL maximum emission intensity is related to the effects of structural order and disorder in the material which result in different electron transfer processes due to different distributions of intermediate levels of energy between the VB and CB. Studies of molybdates PL [1] suggest that distorted clusters of $[MoO_3]$ and $[MoO_4]$ in the network lead to the formation of intermediate levels

of energy within the band gap. These energy levels are basically composed of oxygen 2p states (near the valence band) and Mo 4d states (below the conduction band). In these cases, polarizations induce a symmetry breaking and localized energy levels that favor the trapping of electrons. For $CoMoO_4$ powders synthesized in this study, the ratio of order and disorder can result from the interaction of microwave energy with $[MoO_3]$ and $[MoO_4]$ clusters. The interaction of these clusters with microwave radiation produces the formation of defects and/or distortions in these materials.

The α- and β-$CoMoO_4$ nanorods have a broad band emission typical of systems where relaxation processes occur by different paths which involve intermediary levels in the "band gap". Thus, the decomposition of these broad bands (see **Figure 10**) was used to obtain information on the PL response influenced by electronic transitions. The decomposition was performed using the Peak-Fit Program (version 4.05), and the Gaussian function was used successfully to fit the PL peaks and tuning parameters, including peak positions and corresponding areas (see **Table 2**). In this study, PL curves can be composed of three components: 1) the blue component (with a maximum at around 440 nm); 2) the blue-green component (with a maximum at around 475 nm); and the green component (with a maximum at around 525 nm). An analysis of the evolution of the PL emission of D1,
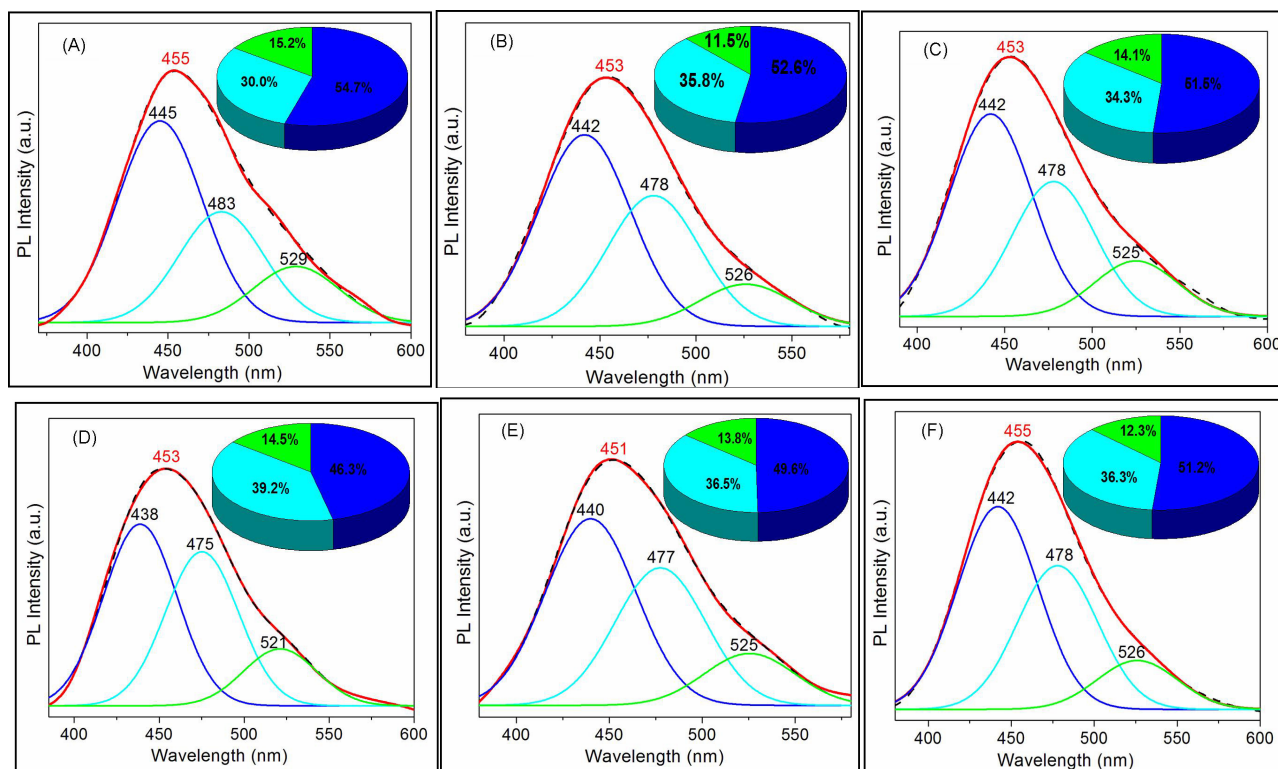

Figure 10. Deconvolution of the PL spectra of for the samples α- and β-CoMoO₄: (A) D1, (B) D2, (C) D4, (D) D8, (E) D16 and (F) D32.

ACES

Table 2. Data obtained by the decomposition of PL bands of α- and β-CoMoO$_4$ samples.

Sample	PL emission maximum (nm)	Peak 1		Peak 2		Peak 3	
		λ (nm)	Área (%)	λ (nm)	Área (%)	λ (nm)	Área (%)
D 1	455	445	54.7	483	30.0	529	15.2
D 2	453	442	52.5	478	35.8	526	11.5
D 4	453	442	51.5	478	34.3	525	14.1
D 8	453	438	46.2	475	39.2	521	14.5
D 16	451	440	49.6	477	36.5	525	13.8
D 32	455	442	51.2	478	36.3	526	12.3

D2, D4, D8 D16 and D32 powders (see **Table 2**) reveals that all samples exhibit a PL emission maximum at *ca.* 455 nm (blue emission) which indicates that the charge transference process as well as the trapping of electrons occurs because of a greater contribution of shallow holes rather than deep holes[33].

4. Conclusion

A synthesis process utilizing the MAH method for a short time was successful in obtaining precursors of both α- and β-CoMoO$_4$ Nanorods. XRD patterns and Raman spectra at room temperature showed that these powders have both α and β phases related to the CoMoO$_4$ with a space group of C2/m. These materials contain nanorod morphologies, and all samples exhibit a PL emission maximum at *ca.* 455 nm (in the blue emission) which indicates that the charge transference process as well as the trapping of electrons occurs because of a greater contribution of shallow holes rather than deep holes.

5. Acknowledgements

REFERENCES

[1] A. P. A. Marques, V. M. Longo, D. M. A. de Melo, P. S. Pizani, E. R. Leite, J. A. Varela and E. Longo, "Shape Controlled Synthesis of CaMoO$_4$ Thin Films and Their Photoluminescence Property," *Journal of Solid State Chemistry*, Vol. 181, No. 5, 2008, pp. 1249-1257. doi:10.1016/j.jssc.2008.01.051

[2] N. Klassen, S. Shmurak, B. Red'kin, B. Ille, M. Lebeau, P. Lecoq and M. Schneegans, "Correlations between Structural and Scintillation Characteristics of Lead and Cadmium Tungstates," *Nuclear Instruments and Methods in Physics Research Section A*: *Accelerators*, *Spectrometers*, *Detectors and Associated Equipment*, Vol. 486, No. 1-2, 2002, pp. 431-436. doi:10.1016/S0168-9002(02)00748-9

[3] F. A. Danevich, A. S. Georgadze, V. V. Kobychev, B. N. Kropivyansky, V. N. Kuts, A. S. Nikolaiko, V. I. Tretyak and Y. Zdesenko, "The Research of 2β Decay of ^{116}Cd with Enriched ^{116}CdWO$_4$ Crystal Scintillators," *Physics Letters B*, Vol. 344, No. 1-4, 1995, pp. 72-78. doi:10.1016/0370-2693(94)01528-K

[4] B. G. Hyde and S. Andersson, "Inorganic Crystal Structures," *Crystal Research and Technology*, Vol. 25, 1990, p. 676.

[5] A. P. Young and C. H. Schwartz, "High-Pressure Synthesis of Molybdates with the Wolframite Structure," *Science*, Vol. 141, No. 3578, 1963, pp. 348-349. doi:10.1126/science.141.3578.348

[6] Y. Ding, Y. Wan, Y. L. Min, W. Zhang and S. H. Yu, "General Synthesis and Phase Control of Metal Molybdate Hydrates MMoO$_4$·nH$_2$O (M = Co, Ni, Mn, n = 0, 3/4, 1) Nano/Microcrystals by a Hydrothermal Approach: Magnetic, Photocatalytic, and Electrochemical Properties," *Inorganic Chemistry*, Vol. 47, No. 17, 2008, pp. 7813-7823. doi:10.1021/ic8007975

[7] J. E. Miller, N. B. Jackson, L. Evans, A. G. Sault and M. M. Gonzales, "The Formation of Active Species for Oxidative Dehydrogenation of Propane on Magnesium Molybdates," *Catalysis Letters*, Vol. 58, No. 2-3,1999, pp. 147-152. doi:10.1023/A:1019013514105

[8] J. A. Rodriguez, S. Chaturvedi, J. C. Hanson and J. L. Brito, "Reaction of H$_2$ and H$_2$S with CoMoO$_4$ and NiMoO$_4$: TPR, XANES, Time-Resolved XRD, and Molecular-Orbital Studies," *Journal of Physical Chemistry B*, Vol. 103, No. 5, 1999, pp. 770-781. doi:10.1021/jp983115m

[9] J. Zhao, Q. Wu and M. Wen, "Temperature-Controlled Assembly and Morphology Conversion of Co MoO$_4$·3/4 H$_2$O Nano-Superstructured Grating Materials," *Journal of Materials Science*, Vol. 44, No. 23, 2009, pp. 6356-6362. doi:10.1007/s10853-009-3876-y

[10] K. Eda, Y. Uno, N. Nagai, N. Sotani and M. S. Whittingham, "Crystal Structure of Cobalt Molybdate Hydrate CoMoO$_4$·nH$_2$O," *Journal of Solid State Chemistry*, Vol. 178, No. 9, 2005, pp. 2791-2797. doi:10.1016/j.jssc.2005.06.014

[11] J. A. Rodriguez, S. Chaturvedi, J. C. Hanson, A. Albornoz and J. L. Brito, "Electronic Properties and Phase Transformations in CoMoO$_4$ and NiMoO$_4$: XANES and Time-Resolved Synchrotron XRD Studies," *Journal of Physical Chemistry B*, Vol. 102, No. 8, 1998, pp. 1347-1355. doi:10.1021/jp972137q

[12] H. Ehrenberg, M. Wiesmann, J. García-Jaca, H. Weitzel and H. Fuess, "Magnetic Structures of the High-Pressure

Modifications of CoMoO$_4$ and CuMoO$_4$," *Journal of Magnetism Materials*, Vol. 182, No. 1-2, 1998, pp. 152-160. doi:10.1016/S0304-8853(97)01008-1

[13] Y. M. Kong, J. Peng, Z. F. Xin, B. Xue, B. X. Dong, F. S. Shen and L. Li, "Selective Synthesis and Novel Properties of Single Crystalline α-CoMoO4 Nanorods/Nano Whiskers," *Materials Letters*, Vol. 61, No. 10, 2007, pp. 2109-2112. doi:10.1016/j.matlet.2006.08.028

[14] M. Wiesmann, H. Ehrenberg, G. Wltschek, P. Zinn, H. Weitzel and H. Fuess, "Crystal Structures and Magnetic Properties of the High-Pressure Modifications of Co-MoO$_4$ and NiMoO$_4$," *Journal of Magnetism of Magnetism Materials*, Vol. 150, No. 1, 1995, pp. L1-L4. doi:10.1016/0304-8853(95)00516-1

[15] Y. Y. Meng and Z. X. Xiong, "Preparation of Molybdates with Antibacterial Property," *Key Engineering Materials*, Vol. 368-372, 2008, pp. 1516-1518. doi:10.4028/www.scientific.net/KEM.368-372.1516

[16] C. Mazzocchia, C. Aboumrad, C. Diagne, E. Tempesti, J. M. Herrmann and G. Thomas, "On the NiMoO$_4$ Oxidative Dehydrogenation of Propane to Propene: Some Physical Correlations with the Catalytic Activity," *Catalysis Letters*, Vol. 10, No. 3-4, 1991, pp.181-191. doi:10.1007/BF00772070

[17] J. L. Brito and A. L. Barbosa, "Effect of Phase Composition of the Oxidic Precursor on the HDS Activity of the Sulfided Molybdates of Fe(II), Co(II), and Ni(II)," *Journal of Catalysis*, Vol. 171, No. 2, 1997, pp. 467-475. doi:10.1006/jcat.1997.1796

[18] G. W. Smith, "The Crystal Structures of Cobalt Molybdate CoMoO$_4$ and Nickel Molybdate NiMoO$_4$," *Acta Crystallographica*, Vol. 15, 1962, pp. 1054-1057. doi:10.1107/S0365110X62002765

[19] A. W. Sleight and B. L. Chamberland, "Transition Metal Molybdates of the Type AMoO$_4$," *Inorganic Chemistry*, Vol. 7, No. 8, 1968, pp. 1672-1675. doi:10.1021/ic50066a050

[20] K. Sieber, R. Kershae, K. Dwight and A. Wold, "Dependence of Magnetic Properties on Structure in the Systems Nickel(II) Molybdate(VI) and Cobalt(II) Molybdate(VI)," *Inorganic Chemistry*, Vol. 22, No. 19, 1983, pp. 2667-2669. doi:10.1021/ic00161a004

[21] C. Mazzocchia, C. Aboumrad, C. Diagne, E. Tempesti, J. M. Herrmann and G. Thomas, "On the NiMoO$_4$ Oxidative Dehydrogenation of Propane to Propene: Some Physical Correlations with the Catalytic Activity," *Catalysis Letters*, Vol. 10, No. 3-4, 1991, pp. 181-191.

[22] A. Maione and M. Devilers "Solid Solutions of Ni and Co Molybdates in Silica-Dispersed and Bulk Catalysts Prepared by Sol-Gel and Citrate Methods," *Journal of Solid State Chemistry*, Vol. 177, No. 7, 2004, pp. 2339-2349. doi:10.1016/j.jssc.2004.03.022

[23] J. Bi, C.-H. Cui, X. Lai, F. Shi and D.-J. Gao, "Synthesis

of Luminescent SrMoO$_4$ Thin Films by a Non-Reversible Galvanic Cell Method," *Materials Research Bulletin*, Vol. 43, No. 3, 2008, pp. 743-747. doi:10.1016/j.materresbull.2007.03.021

[24] S. Komarneni, R. Roy and Q. H. Li, "Microwave-Hydrothermal Synthesis of Ceramic Powders," *Materials Research Bulletin*, Vol. 27, No. 12, 1992, pp. 1393-1405. doi:10.1016/0025-5408(92)90004-J

[25] S. Komarneni, Q. H. Li and R. Roy, "Microwave-Hydrothermal Processing for Synthesis of Layered and Network Phosphates," *Journal of Materials Chemistry*, Vol. 4, 1994, pp. 1903-1906. doi:10.1039/jm9940401903

[26] G. J. Wilson, A. S. Matijasevich, D. R. G. Mitchell, J. C. Schulz and G. D. Will, "Modification of TiO$_2$ for Enhanced Surface Properties: Finite Ostwald Ripening by a Microwave Hydrothermal Process," *Langmuir*, Vol. 22, No. 5, 2006, pp. 2016-2027. doi:10.1021/la052716j

[27] J. C. Sczancoski, L. S. Cavalcante, M. R. Joya, J. A. Varela, P. S. Pizani and E. Longo, "SrMoO$_4$ Powders Processed in Microwave-Hydrothermal: Synthesis, characterization and Optical Properties," *Chemical Engineering Journal*, Vol. 140, No. 1-3, 2008, pp. 632-637. doi:10.1016/j.cej.2008.01.015

[28] M. Abdel-Dayem Hany, "Dynamic Phenomena during Reduction of α-NiMoO4 in Different Atmospheres: *In-situ* Thermo-Raman Spectroscopy Study," *Industrial & Engineering Chemistry Research*, Vol. 46, No. 8, 2007, pp. 2466-2472. doi:10.1021/ie0613467

[29] L. S. Cavalcante, J. C. Sczancoski, L. F. Lima Jr., J. W. M. Espinosa, P. S. Pizani, J. A. Varela and E. Longo, "Synthesis, Characterization, Anisotropic Growth and Photoluminescence of BaWO$_4$," *Crystal Growth & Design*, Vol. 9, No. 2, 2009, pp. 1002-1012. doi:10.1021/cg800817x

[30] D. L. Wood and J. Tauc, "Weak Absorption Tails in Amorphous Semiconductors," *Physical Review B*, Vol. 5, No. 8, 1972, pp. 3144-3151. doi:10.1103/PhysRevB.5.3144

[31] P. K. Pandey, N. S. Bhave and R. B. Kharat, "Structural, Optical, Electrical and Photovoltaic Electrochemical Studies of Cobalt Molybdate Thin Films," *Indian Journal of Pure & Applied Physics*, Vol. 44, 2006, pp. 52-28.

[32] A. P. A. Marques, F. V. Motta, E. R. Leite, P. S. Pizani, J. A. Varela, E. Longo and D. M. A. de Melo, "Evolution of Photoluminescence as a Function of the Structural Order or Disorder in CaMoO$_4$ Nanopowders," *Journal of Applied Physics*, Vol. 104, No. 4, 2008, Article ID: 043505. doi:10.1063/1.2968388

[33] X. Wu, J. Du, H. Li, M. Zhang, B. Xi, H. Fan, Y. Zhu and Y. Qian, "Aqueous Mineralization Process to Synthesize Uniform Shuttle-Like BaMoO$_4$ Microcrystals at Room Temperature," *Journal of Solid State Chemistry*, Vol. 180, No. 11, 2007, pp. 3288-3295. doi:10.1016/j.jssc.2007.07.010